Aberystwyth University

Massive blow-out craters formed by hydrate-controlled methane expulsion from the Arctic seafloor

Andreassen, K.; Hubbard, Alun; Winsborrow, M.; Patton, H.; Vadakkepuliyambatta, S.; Plaza-Faverola, A.; Gudlaugsson, E.; Serov, P.; Deryabin, A.; Mattingsdal, R.; Mienert, J.; Bünz, S.

Massive blow-out craters formed by hydrate-controlled methane expulsion from the Arctic seafloor

One Sentence Summary: Giant craters formed after Barents Sea deglaciation provide an analogue for future destabilization of subglacial gas hydrates

K. Andreassen[1*], A. Hubbard[1], M. Winsborrow[1], H. Patton[1], S. Vadakkepuliyambatta[1,] A. Plaza-Faverola[1], E. Gudlaugsson[1], P. Serov[1], A. Deryabin[2], R. Mattingsdal[2], J. Mienert[1], S. Bünz[1]

[1]CAGE - Centre for Arctic Gas Hydrate, Environment and Climate, Department of Geosciences, UiT – The Arctic University of Norway, N-9037 Tromsø, Norway

[2]Norwegian Petroleum Directorate, Harstad, Norway

*Correspondence to: karin.andreassen@uit.no

Abstract:

Widespread methane release from thawing Arctic gas hydrates is a major concern, yet the processes, sources and fluxes involved remain unconstrained. We present geophysical data documenting a cluster of kilometer-wide craters and mounds from the Barents Sea floor associated with large-scale methane expulsion. Combined with ice sheet/gas hydrate modeling, our results indicate that during glaciation, natural gas migrated from underlying hydrocarbon reservoirs and was sequestered extensively as subglacial gas hydrates. Upon ice sheet retreat, methane from this hydrate reservoir concentrated in massive mounds before being abruptly released to form craters. We postulate that these processes have been widespread during previous glaciations, and provide an analogue for the future destabilization of glacially influenced hydrate reservoirs across continental margins in the Arctic, Antarctic and elsewhere.

Arctic continental shelves and land areas host vast amounts of methane trapped as hydrates - an ice-like, solid mixture of gas and water (*1, 2*). Methane is a potent greenhouse gas, and sustained warming in the Arctic (*3*) has increased awareness that future destabilization of these shallow carbon reservoirs could cause a positive feedback to climate warming (*4*). Methane hydrate is stable within sub-seafloor sediments on continental margins worldwide, typically where water depths exceed 300 m and water temperatures are lower than around 5°C, whilst hydrates of heavier hydrocarbons are found at even shallower depths (*5*). Extensive gas hydrates also exist below permafrost on shallow Arctic continental shelves and land areas (*1*). Ice, permafrost and gas hydrates combine to form a cryospheric cap that acts to trap natural gas leaking from underlying hydrocarbon reservoirs (*6*).

High levels of methane emissions from decomposing gas hydrates have been observed on the East Siberian Arctic Shelf (7) and on upper continental slopes worldwide (*2*), but there is no

documented evidence that they impact on the atmosphere (*2*). However, there is a large difference between slow, steady degassing (e.g., *9*) and the sudden, high-magnitude degassing events like those that formed the large blow out craters on the Russian Arctic Yamal and Gydan Peninsulas (*10, 11*). Slow methane seepage from under 200 m of water or on land does not appreciably contribute to the atmosphere as most of the methane is oxidized or dissolved into the sediments or water column (*2*), whereas abrupt blow-outs could eject massive fluxes of methane into the atmosphere. Such large methane-discharging craters, inferred to result from decomposing gas hydrates, have been reported both from Arctic marine (*12, 13*) and land areas (*10, 11*), but little is known about their formation.

Here, we revisit a cluster of kilometer-wide craters in the northern Barents Sea (Fig. 1) inferred to have formed after deglaciation of the area around 15,000 years ago (*12, 13*), to elucidate the processes and mechanisms of their formation. The investigation is based on new geophysical data from the subsurface, the seafloor and water column, integrated with numerical modeling of the hydrate stability zone over the past 30,000 years spanning full glacial to inter-glacial conditions (*14*). In the model, transient evolution of the hydrate system is determined by the diffusive heat transport through sediments and ice, subglacial and seafloor temperature variations, ice thickness, isostatic loading, and eustatic sea level variations (*14*).

The study site is located within the Polar North Atlantic, in northern Bjørnøyrenna (Bear Island Trough) on the contemporary methane hydrate stability boundary (Fig. 1A). The seafloor is generally smooth, sloping from 310 m below sea level (mbsl) in the north to 370 mbsl in the south (Fig. 1B). The Barents Sea was extensively glaciated by a marine-based ice sheet that attained its peak during the Last Glacial Maximum (LGM) ~23,000 years before present (BP) (Fig. 1A). On retreat, the NW sector of this ice sheet experienced a stepwise retreat through Bjørnøyrenna with

the study site deglaciating around 15,000 years BP (*15, 16*. The giant craters and mounds (Fig. 1B) are etched into sedimentary bedrock of Middle-Triassic age and are located on the western flank of a large anticline (Fig. S1C). Extensive erosion throughout the Cenozoic has cut this stratigraphic structural high down to a series of well-developed clinoforms (Fig. S1A). The topsets of these clinoforms have high potential for sands where fluids can migrate (*17*), whilst the bottom-sets are an organically rich source of hydrocarbon fluids (*18*). A strategic petroleum industry borehole (Fig. S1A; 7427/3-U-01) documents lithologies consisting predominantly of shale, coarsening upwards into layers of fine sandstone (*18*). Seismic profiling indicates a series of faults and fractures leading upwards from the Triassic hydrocarbon source and reservoir rocks directly into the seafloor craters and mounds (Fig. S2C).

High-resolution bathymetry reveals over 100 giant craters within a 440 km^2 area of the seafloor (Fig. 1B). The craters are generally oval in shape, between 300 and 1000 m in diameter and up to 30 m deep. Many have steep walls with gradients up to 50° but lack berms at their sides (e.g., Figs. 2A and 2B; C3, C4, C5). Others have a more complex morphology, typically with gently dipping sides and often contain one or more internal mounds (e.g., Fig. 2A; C1, C2). Analysis of chirp- and seismic-profiles verified against sediment cores, reveals unlithified seafloor sediments to be less than 2 m thick. Numerous large seafloor mounds are also identified, mainly located at the flanks of the giant craters (Fig. 2B; M1 and M3). These mounds are up to 1100 m wide and 20 m high, are generally semi-circular to elliptical in plan-form, steep-sided, and have an irregular upper surface incised with straight or curved furrows (Fig. S2D; M1 to M6). Some of the furrows are iceberg scours, while others are associated with sub-cropping fractures and erosion pits formed by gas escape along faults and fractures. Smaller craters and mounds between 50 and 200 m wide with varying relief are abundant across the study site, clustered around and within the larger craters (Fig. 2, Figs. S2B and S2D).

Over 600 gas flares are identified as water column acoustic anomalies in echo-sounder profiles (Fig. 2A; red to yellow columns) due to strong velocity/density contrasts between chains of gas bubbles and the water-column. Single flares are typically 50 to 200 m wide and rise to ~200 m into the water column (Fig. 2A). The majority of flares emerge around and between craters and mounds, whereas some originate from within the craters and mounds themselves (Fig. 2). We interpret the presence of strong seismic reflections with a phase-reversed polarity compared to seafloor reflections as free gas accumulations in the sub-seafloor sediments (*19*; e.g. Fig. 2B). Such free gas accumulations are observed in vertical zones (gas chimneys) with high-amplitude, chaotic seismic reflection patterns below the craters (Fig. 2A). These chimneys appear where natural gas distributes into irregular patches in fractured, low-permeable shales (*19*).

Measurements acquired directly from seafloor sediments (Fig. 2) indicate that 87% of the gas present at mound M1 is methane, with 12% ethane and propane (Table S1; GC 1202). Due to its heavier hydrocarbon content, this natural gas is stable as structure II hydrates (*5*) under present seafloor depth and temperature conditions (Fig. 3A; purple line year 0). However, gas sampled from crater C7 is almost pure methane, with just 0.1% heavier hydrocarbon and hence, is unstable in hydrate form under present seafloor conditions (Fig. 3; black stippled line). Analysis of gas ratios (Table S2) indicates a thermogenic origin for the natural gas and associated hydrates, where organic molecules are broken down under high-temperature, high-pressure conditions at subsurface depths typically exceeding 1 km (*20*).

As the observed mounds are elevated well above the surrounding seafloor, any plausible formation mechanism must either deposit material on the existing seafloor, or otherwise uplift the existing sedimentary bedrock. The absence of any discernible seismic paleo-seafloor reflections from the base of the mounds (e.g., Fig. 2B; M1) and a distinct lack of extrusive features such as mud flows and mud cones, discounts extrusive processes (*21*). Ejecta deposits sourced from the

adjacent craters (*12*) would likewise have a clear basal reflection, as would carbonate and/or coral

mounds (*22*). The lack of a basal reflector, combined with the presence of actively venting natural

gas connected to deeper hydrocarbon sources, leads us to assert that the giant mounds we observe

are formed by the expansion of gas hydrate accumulations within the subsurface. Similar but

smaller mounds have been observed elsewhere and are often referred to as gas hydrate pingos

(e.g., *21*).

We propose a conceptual model that links the formation of these hydrate pingos with the

giant craters through the buildup and subsequent dissociation of gas hydrates (Fig. 3). Cyclic

episodes of Barents Sea ice sheet loading and unloading throughout the Pleistocene, caused

repeated pressurization and depressurization of the underlying thermogenic hydrocarbon

reservoirs. This would have driven large fluxes of natural gas upwards into the near subsurface

(*23*), with gas migration focused into the crater and mound area by the morphology of the deeper

Middle Triassic anticline structure (Figs. S1A and S1C). Subglacial conditions associated with a

~2 km thick ice sheet during the LGM (*14*) acted to stabilize methane hydrate formation within

the upper ~440 m of sub-seafloor sediments (Fig. 3A; orange line). Heavier hydrates were stable

down to around 520 m (Fig. 3A; green line). Lateral sequestration of gas hydrates within the

coarse-grained porous bedrock were accompanied by free natural gas accumulating in faults and

fractures below the hydrate stability zone (Fig. 3B).

The rapid transition of the seafloor from a subglacial to marine environment when the ice sheet

retreated, abruptly degraded conditions conducive for hydrate stability, forced by a dramatic

reduction in loading, hydrostatic pressure and increase in temperature (Fig 3B). Between 17,000

and 15,000 years ago the gas-hydrate stability zone diminished from ~440 to ~200 m (Fig. 3A;

BGHZ curves), causing deeper hydrates to decompose, migrate upwards and recrystallize at

shallower depths (*14*). This resulted in an increased volume of gas concentrated within a

progressively thinning and shallowing gas hydrate stability zone. This volume expansion due to gas hydrate re-growth, along with accumulations of underlying pressurized free gas, led to the development of the gas hydrate pingos (Fig. 3C; e.g., *21*). Driven by ongoing isostatic rebound and inflow of warm North Atlantic water (*26*), the methane hydrate stability zone continued to thin to ~30 m by 12,000 yr BP (Fig. 3A; orange and black stippled lines), despite eustatic sea level rise. Finally, the release of gas from decomposed hydrate accumulations drove hydrofractures through the overburden rocks and sediment, triggering multiple methane-release events and creating ballistic gas expulsions. These expulsion events eroded and deformed the fractured sediments, promoting overlying seafloor blow-out and the formation of the massive craters observed today (e.g., *24*; Fig. 3D).

The appearance of gas chimneys under most of the craters and gas flares around and on the flanks of craters (Fig. 2) implies that upward gas migration pathways through the craters became partially blocked. The plugging of gas flow pipes after blow-out, and formation of new pipes adjacent to old ones to release rising gas pressure, have been suggested in other blow-out settings (*24*). When combined, these processes explain the development of the system of giant craters with underlying, interconnected pipes and the distribution of smaller mounds and craters on the flanks of the larger craters (Fig. 3E) that act to promote further crater expansion (Fig. 2).

The craters and mounds cut across, and therefore post-date mega-scale glacial lineations (MSGLs) - landforms developed beneath the fast-flowing Bjørnøyrenna ice stream (*15*) (Fig. S2D; black lines). Iceberg ploughmarks are also observed to erode and incise the tops of mounds, with some tracking down into and across craters (Fig. S2D; stippled white lines) signifying that the craters and mounds formed whilst icebergs with keels between 300 and 400 m deep were active in the Barents Sea. We can hence constrain the timing of crater and mound formation to a relatively short time window after the onset of local ice-free conditions around 15,000 years BP,

but before or during the final stages of ice stream retreat from northern Bjørnøyrenna around

11,600 years ago (*25*). This chronology is entirely consistent with our modeling of the rapid

thinning of the methane hydrate stability zone from 15,000 to 12,000 years, with the final stages

of decomposition complete by 11,000 years ago (Fig. 3A; orange and stipple-black lines).

The primary drivers for gas hydrate dissociation and gas expulsion varied in space and time

over the glaciated Barents Sea, but were critically controlled, either directly or indirectly, by ice

sheet evolution. At the study area, depressurization due to the loss of subglacial loading of ~1950

m thick ice, greatly exceeded any hydrostatic compensation associated with changes in relative

sea level (+115 m eustatic sea level rise and -205 m in isostatic depression) since the LGM. On

deglaciation of our study area, the impact of isostatic loading left the water depth at around 440 m,

still some ~115 m higher than today despite the fact that eustatic sea level was 80 m lower at the

time. The temperate (i.e. at pressure-melting point) subglacial conditions associated with the

Bjørnøyrenna ice stream precluded the development of a thick permafrost horizon even during

LGM conditions (Fig. 3A; permafrost and Fig. S3). Rapid retreat of the actively calving

Bjørnøyrenna ice stream was partially driven by the ingress of relatively warm Atlantic water

(*26*), that also adversely influenced the stability of sequestered seafloor hydrates (Fig. 3A; red

temperature curve).

The presence of active contemporary gas flares demonstrates continued slow methane

release across the study area. Geological analogues of slow and sustained, fluid-flow events

southwest of the area have recently been dated using authigenic carbonate crusts. Here, methane

release commenced after the ice sheet retreated and continued for up to 10,000 years (*27*) at flow

rates of 20 to 60 cm per year (*28*). Our analysis suggests that glaciated petroleum provinces are

preconditioned to sequester large fluxes of methane subglacially, in extensive, but

heterogeneously distributed, gas hydrate accumulations. On ice sheet retreat, these gas hydrates

dissociate, forming surface expressions such as gas hydrate pingos, which eventually collapse into craters, releasing large fluxes of methane. Gas hydrate pingos are some of the most climatically sensitive settings as they often contain shallow and relatively pure methane hydrate (*29*) that can dissociate rapidly in response to even moderate environmental perturbations (*30*).

The gas stored within the Bjørnøyrenna pingos accumulated until it over-pressurized and subsequently vented ballistically, releasing massive volumes of methane into the water column that likely attained the atmosphere. Major methane venting events analogous to this appear to be rare, but may easily be overlooked due to high rates of post-glacial deposition limiting their exposure in the geological record. Identification of craters of similar size and morphology as those identified in this study, on buried glacial surfaces farther south in the Barents and North Seas (*31, 32*; Fig. 4; green dots), supports this proposition. Despite their apparent infrequency, the net impact of such high magnitude blow-out events may still be greater than the sustained but gradual seepage, for which the geological record reveals abundant evidence (*2, 8, 27*).

Seafloor craters and/or hydrate mounds are commonly associated with gas seepage at petroleum provinces elsewhere, such as the Gulf of Mexico (*33, 29, 34*) and the West African continental margin of Congo (*35*), Nigeria (*24*) and Angola (*21*). Many of these features are similar to those at our study site and are also related to seafloor doming and blow-out by over-pressured natural gas. However, in these warm oceanic settings, the seafloor is often several thousand m deep and associated with sub-seafloor gas hydrates that are deeply buried. Here, we propose a new conceptual model that links large-scale seafloor methane expulsion to processes related to ice sheet retreat with implications for future destabilization of shallow, high-latitude gas hydrate systems.

Many thermogenic gas reservoirs have been confirmed, and more are evident beneath formerly glaciated continental margins across the Arctic (Fig. 4; pink to dark red areas) and

elsewhere. There are presently over 33 million km^2 of glaciated continental margins (*36*) that coincide with confirmed hydrocarbon reserves off USA, Canada, Russia, NW Europe (*37, 14*). During glaciation, this vast tract would have experienced ideal high-pressure/low-temperature subglacial conditions for extensive sequestration of methane and heavier gases in hydrate form. Analogous to this study, such methane hydrates would subsequently have been subject to similar deglaciation-triggered decomposition, release and catastrophic expulsion into the water-column, and potentially, the atmosphere.

This study reveals that large-scale, hydrate-controlled methane expulsions from the Arctic seafloor took place at a time when the Earth was warming in line with large increases in atmospheric methane (*4, 38*). There is abundant evidence that much of the methane sustaining this abrupt period of warming originated from wetlands (*39*), but outbursts of methane from decomposing hydrates and underlying gas accumulations could also have played an important role (*4*). The conceptual model presented in this study (Fig. 3) delivers a benchmark for the destabilization and release of glacially influenced gas-hydrate reservoirs that have the potential to impact on global atmospheric composition and hence climate, not only in the past but also the future, since it is apparent that extensive subglacial hydrate accumulations exist beneath the Antarctic and Greenland ice sheets today (*40, 6*).

References and Notes

1. K. A. Kvenvolden, *Chem. Geol.* **71**, 41-51 (1988).

2. C.D. Ruppel, J.D. Kessler, Rev. Geophys. 55, doi:10.1002/2016RG000534 (2017).

3. IPCC, The Physical Science Basis. Contribution of Working Group I. In *Fifth Assessment Report of the Intergovernmental Panel on Climate Change*, T. F. Stocker *et al.*, Eds. Cambridge Univ. Press (2013).

4. E.G. Nisbet, J. Chappellaz, *Science* **324**, 477-478 (2009).

5. E. D. Sloan, C. A. Koh, *Clathrate hydrates of natural gases* (Boca Raton, Florida, ed. 3, 2008).

6. K. M. Walter Anthony, P. Anthony, G. Grosse, J. Chanton, *Nature Geoscience* **5**, 419-426 (2012).

7. N. Shakova, I. Semiletov, A. Salyuk, V. Yusupov, D. Kosmach, Ö. Gustavsson, *Science* **327**, 1246-1250 (2010).

8. E.G. Nisbet, E.J. Dlugokencky, P. Bousquet, *Science* **343**, 493-495 (2014).

9. G.K. Westbrook, K.E. Tatcher, E.J. Rohling, A.M., Pietrowski, H. Pälike, A.H. Osborne, E.G. Nisbet, T.A. Minshull, M. Lanoisellè, R.H. James, V. Hühnerbach, D. Green, R.E. Fisher, A.J. Crocjer, A. Chabert, C. Bolton, A. Beszczynzka-Möller, C. Berndt, A. Aquilinia, *Geophys. Res. Lett.* **36**, L15608 (2009).

10. V. Bogyavleski, *GEO ExPro*, **12** (5), 75-78 (2015). http://www.geoexpro.com/articles/2015/12/gas-blowouts-on-the-yamal-and-gydan-peninsulas

11. M.O. Leibman, A.I. Kizyakov, A.V. Plekhanov, I.D. Streleskaya, *Geography, Environment, Sustainability* **07** (04), 68-80 (2014). http://www.geogr.msu.ru/GESJournal/contents.php?iid=22&menupos=7

12. A. Solheim, A. Elverhøi, *Geo-Marine Letters* **13**, 235-243 (1993).

13. S. Lammers, E. Suess, M. Hovland, *Geol. Rundsch.* **84**, 59-66 (1995).

14. Materials and Methods are available as Supplementary Materials on Science Online

15. M. C. M., Winsborrow, K. Andreassen, G. Corner, J. S. Laberg, *Quaternary Science Reviews* **29**, 424-442 (2010).

16. H. Patton, A. Hubbard, K. Andreassen, M. Winsborrow, A. P. Stroeven, *Quaternary Science Reviews*, 153, 97-121 (2016).

17. T. Høy, B. A. Lundschien, Triassic deltaic sequences in the northern Barents Sea. *Geological Society, London, Memoirs* **35**, 249-260 (2011).

18. B. A. Lundschien, T. Høy, A. Mørk, *Norwegian Petroleum Directorate Bulletin* **11**, 3-20 (2014).

19. H. Løseth, M. Gading, L. Wenasas, *Mar. Petrol. Geol.* **26**, 1304-1319 (2009).

20. K. A. Kvenvolden, T. M. Vogel, J. V. Gardner, *Journal of Geochemical Exploration* **14**, 209-219 (1981).

21. C. Serié, M. Huuse, N.S. Schødt, *Geology* **40**, 207-210 (2012).

22. E. Le Guilloux, K. Olu, J. F. Bourillet, B. Savoye, S. P. Iglésias, M. Sibuet, *Deep-Sea Research Part II: Topical Studies in Oceanography* **56**, 2394-2403 (2009).

23. I.Yu, Z. Lerche, B. Torudbakken, R.O. Thomsen, *Mar. Petrol. Geol.* **14**, 277-228 (1997).

24. H. Løseth, L. Wensaas, B. Arntsen, N.-M. Hanken, C. Basire, K. Graue, *Mar. Petrol. Geol.* **28**, 1047-1060 (2011).

25. K. Andreassen, M. C. M. Winsborrow, L. R. Bjarnadóttir, D. C. Rüther, *Quaternary Science Reviews* **92**, 246-257 (2014).

26. D. K. Kristensen, T. L. Rasmussen, N. Koç, *Boreas* **42**, 798–813 (2013).

27. A. Crémièr, A. Lepland, S. Chyans, D. Sahy, D. J. Condon, S. R. Noble, M. Tönu, T. Thorsnes, S. Sauer, H. Brunstad, *Nature Communications* 10.1038/ncomms11509 (2016).

28. R. Luff, K. Wallmann, G. Aloisi, *Earth Plant. Sci. Lett.* **221**, 337-353 (2004).

29. I. R. MacDonald, N.L. Guinasso Jr., R. Sassen, J.M. Brooks, L. Lee, K. T. Scott, *Geology* **22**, 699-702 (1994).

30. C. D. Ruppell, *Nature Education Knowledge* **3**(10): 29 (2011).

31. I. Ostanin, Z. Anka, R. di Primo, A. Bernal, *Mar. Petrol. Geol.* **43**, 127-146 (2013).

32. C. Fiechler, S. Henriksen, H. Rueslaatten, M. Hovland, *Petroleum Geoscience* **11**, 331-337 (2005).

33. D.B. Prior, E.H. Doyle, M.J. Kaluza, *Science* **243**, 517-519 (1989).

34. F.J. Rocha-Legorreta, *The Leading Edg*e June, 714-717 (2009).

35. A. Gay, M. Lopez, C. Berndt, M. Séranne, *Marine Geology* **244**, 68-92 (2007).

36. J. Ehlers, P.L. Gibbard, *Quaternary International* **164-165**, 6-20 (2007).

37. D. L. Gautier, K. J. Bird, R. R. Charpentier, A. Grantz, D. W. Houseknecht, T. R. Klett, T. E. Moore, J. K. Pitman, C. J. Schenk, J. H. Schuenemeyer, K. Sørensen, M. E. Tennyson, Z. C. Valin, C. J. Wandrey, *Science* **324**, 1175-1179 (2009).

38. E.G. Nisbet, *Can. Jour. Earth Science* **27**, 148-157 (1990).

39. V.V. Petrenko, A.M. Smith, E. J. Brook, D. Lowe, K. Riedel, G. Brailsfjord, Q. Hua, H. Schaefer, N. Reeh, R.F. Weiss, D. Etheridge, J.P. Severinghaus, *Science* **324**, 506-508 (2009).

40. J. L. Wadham, S. Arndt, Tulaczyk, M. Stibal, M. Tranter, J. Telling, G. P. Lis, E. Lawson, A. Ridgwell, A. Dubnick, M. J. Sharp, A. M. Anesio, C. E. H. Butler, *Nature* **288**, 633-637 (2012).

Figure Legends

Fig. 1. Giant craters and mounds are located in the northern Barents Sea. (A) The Barents Sea Ice Sheet reached the continental shelf break during the Last Glacial Maximum (LGM; *16*). Methane hydrate is currently stable in the deepest part of Bjørnøyrenna and other troughs of the Barents Sea (red polygons). **(B)** Giant craters and mounds within the local area of the study site. The black stippled polygon shows previous investigations of the area (*12, 13*). White circles indicate locations of gas samples shown in Tables S2 and S3.

Fig. 2. Giant craters, mounds, gas flares in the water and gas accumulations in the sediments. (A, B) Shaded relief bathymetry, combined with 2D seismic profiles showing indications of gas in the sediments (phase reversed reflection and gas chimneys). Faults are indicated by brown lines. White circles indicate locations of gas samples shown in Tables S2 and S3.

Fig. 3. Conceptual sketch for formation of craters and mounds in the northern Barents Sea. (A) Numerical model of thickness for the ice sheet (*16*), the gas hydrate stability zone for different gas compositions and subglacial permafrost over the last 30,000 years. The model values are calculated at the location of mound M1 (Fig. 2B). The base of the gas hydrate stability zones (BGHZ) are calculated for gas compositions measured in the seafloor sediments (Table S2) and for pure methane.

(B) Ice loading, focused gas migration along faults and fractures from deeper hydrocarbon reservoirs and formation of subglacial gas hydrate and free gas accumulations. **(C)** The ice sheet retreats and sediment pore pressure is drastically reduced. This leads to decomposition of gas hydrates at depth, build-up of over-pressurized gas below a shallowing gas hydrate zone with increased gas hydrate concentration, and formation of a gas-hydrate pingo. **(D)** Collapse of gas hydrate pingo due to hydrate dissociation, leading to crater formation. **(E)** Collapsed sediments and gas hydrates in the crater

partially block upwards gas flow, which is diverted to the crater flanks. GHSZ: Gas hydrate stability zone.

Fig. 4. Arctic petroleum basins that have been covered by grounded ice during the Quaternary. Areas north of the Arctic Circle with high estimates of undiscovered gas (*37*) that have been covered by a grounded ice sheet during the Quaternary (*36*) are indicated in pink to dark red colors. Gas discoveries in the Barents Sea and North Sea are from the Norwegian Petroleum Directorate (www.npd.no) and the British Government (www.gov.uk/oil-and-gas). Giant craters on the seafloor and buried glaciated surfaces in the Barents Sea (*31*) and North Sea (*32*), as well as craters on land on the Russian Yamal and Gydan Peninsulas (*10)* are indicated.

Acknowledgements

Supplementary Materials

Materials and Methods

Supplementary Text

Figs. S1 to S3

Tables S1 to S3

References and Notes1-40

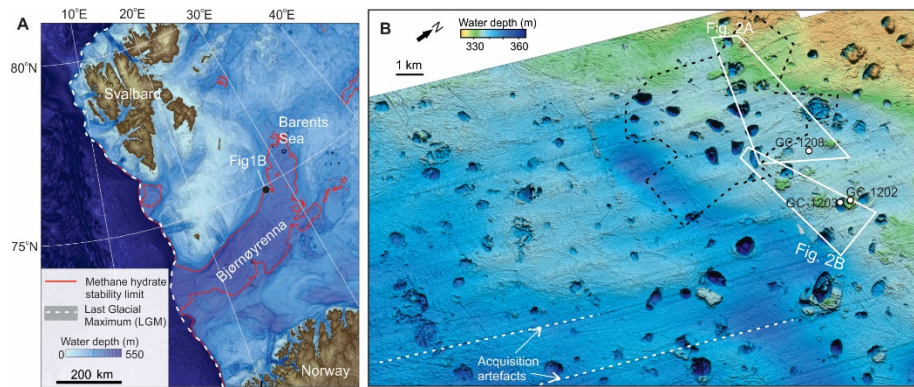References in Supplementary Materials only 41-66

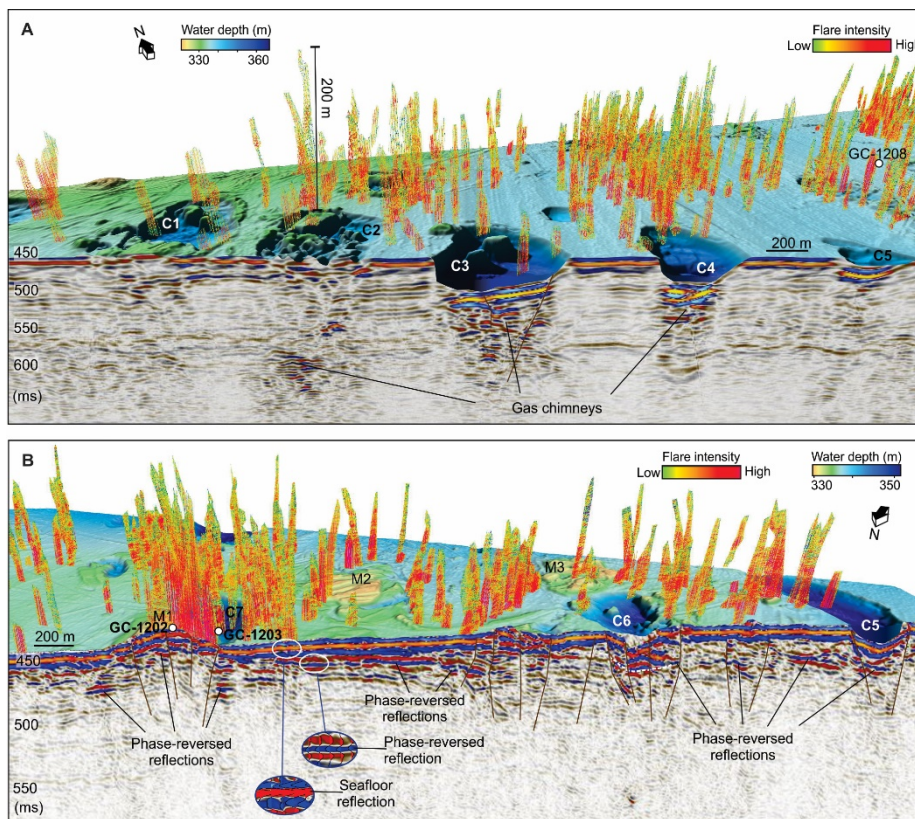Additional Data Table S4 (separate file)
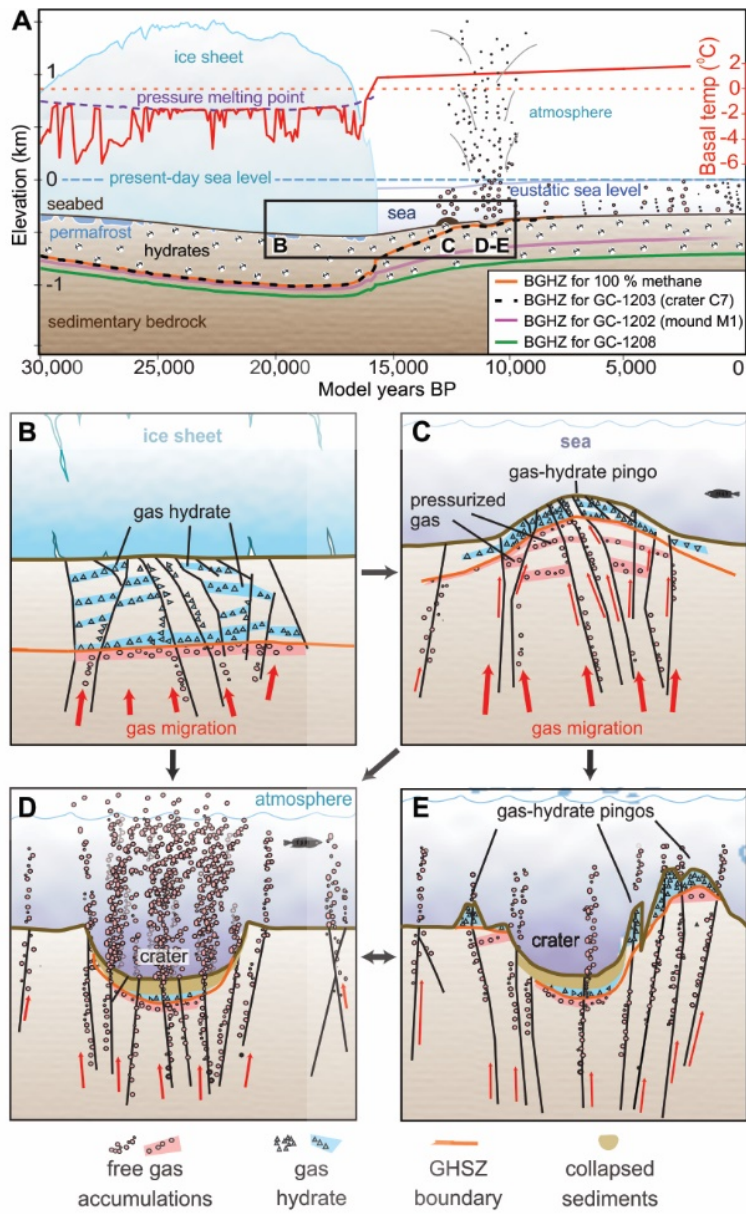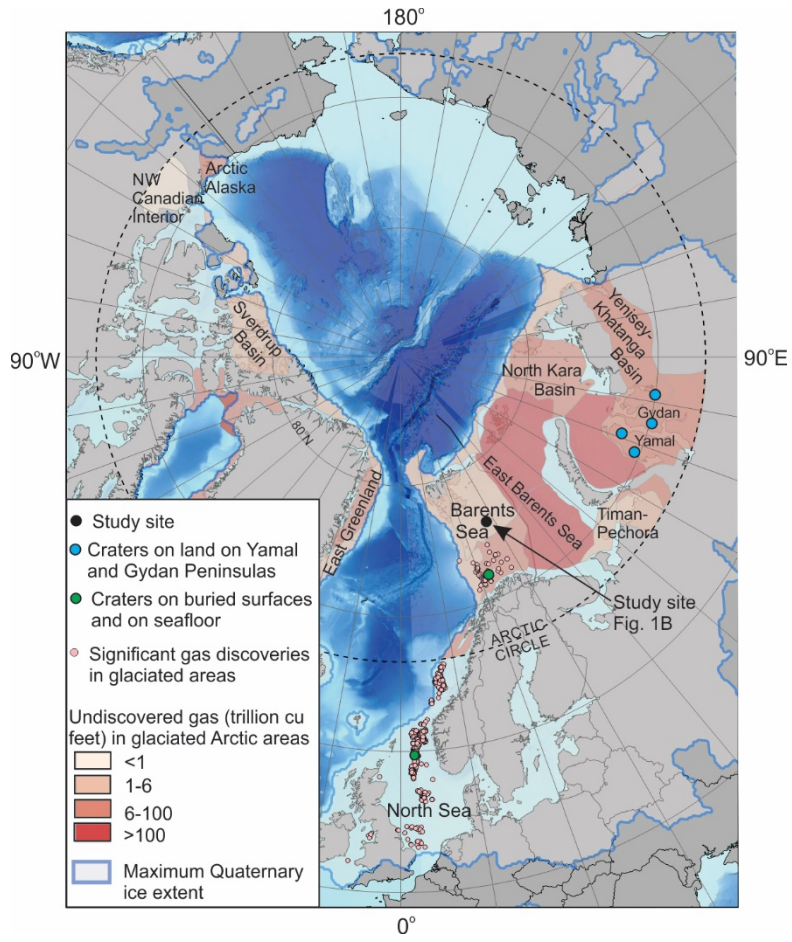
Figures

Fig. 1

Fig. 2

Fig. 3

Fig. 4